

Gas tungsten arc process optimization and assessment for robotized position welding of austenitic stainless steel edge joints

Karhu Miikka, Kujanpää Veli

This is a Author's accepted manuscript (AAM) version of a publication
published by Elsevier
in CIRP Journal of Manufacturing Science and Technology

DOI: 10.1016/j.cirpj.2021.10.012

Copyright of the original publication:

© 2021 CIRP

Please cite the publication as follows:

Karhu, M., Kujanpää, V. (2021). Gas tungsten arc process optimization and assessment for robotized position welding of austenitic stainless steel edge joints. CIRP Journal of Manufacturing Science and Technology, vol. 36, pp. 12-22. DOI: 10.1016/j.cirpj.2021.10.012

**This is a parallel published version of an original publication.
This version can differ from the original published article.**

Gas tungsten arc process optimization and assessment for robotized position welding of austenitic stainless steel edge joints

Miikka Karhu* (miikka.karhu@lut.fi) and Veli Kujanpää (veli.kujanpaa@lut.fi)

Laboratory of Welding Technology, LUT University, Yliopistonkatu 34, 53850, Lappeenranta, Finland

(both authors were earlier with VTT Technical Research Centre of Finland)

*corresponding author

ABSTRACT

Gas tungsten arc welding (GTAW) is a common joining method for austenitic stainless steel sheets. Edge joint is frequently used configuration when the aim is to produce weldments e.g., between the tube sheets and the tubes and to other hollow structures needing tight sealing welds and sound joints. In those applications all positions for welding is usually needed. Robotized welding is utilized, when manual welding is not possible, e.g., in maintenance for nuclear power applications. In automatic welding a strict control of location of arc and welding parameters are extremely important.

In this work the aim was to find suitable welding parameters, as pulse parameters, welding speed and shielding gas composition and study their effects on weld joint penetration and weld quality in different welding positions. In addition, the inaccuracy in the alignment of the arc and its effects was tested in different cases. It was found that it was possible to find the optimal parameters in different positions, flat (PA), overhead (PE), and vertical-up position (PF). However, the vertical-down position (PG) was giving a lower joint penetration in the cases which allow sound welds. Therefore, it was considered that the fabrication of the circumferential joint was best done in two steps to avoid the PG position, which ensures that a sound weld with the set 2.6 mm penetration requirement is achieved over the entire circumference. The use of a shielding gas mixture containing argon and 2% hydrogen showed significant advantages over the other three shielding gas compositions tested, which was observed as deeper penetration of the welds.

Keywords: Gas tungsten arc welding, process optimization, edge joint, robotized position welding, weld joint penetration, austenitic stainless steel

Introduction

Gas tungsten arc welding (GTAW) as well as gas metal arc welding (GMAW) is widely used in joining austenitic stainless steel sheets [1-3]. Gas tungsten arc welding (GTAW), also known as tungsten inert gas (TIG) welding is a gas arc welding process in which an arc burns between an inconsumable tungsten base electrode and a workpiece surrounded by a shielding gas. An overview of arc physics related to GTAW, for example, description of the influence of electrode tip geometry, polarity and the arc fundamentals, can be found in literature references [4-6]. GTAW can be performed either without (i.e., autogenously) or with a filler metal. In the first alternative, the heat of the arc generated by the electrode melts the workpiece into which the weld pool is formed. In the latter alternative, the filler metal in rod or wire form is introduced into the arc generated weld pool either manually or mechanically using a wire feeder [7,8]. Autogenous GTAW is commonly used when the type and fit-up of the joint is such that the mere melting of the base material results in adequate fusion and bead profile of the weld seam. Such examples of the types of joints used are a closed butt joint, a lap joint, a corner joint and also an edge joint, which is also the type of joint used in this work. The weld surface of the gas tungsten arc welded joints is usually smooth and clean in the as-welded condition, so the needs for mechanical surface finishing or other post-weld treatments for the

welds are minimal, for example in the case of certain stainless steels applications being only a chemical pickling treatment.

As with other welding processes, several process variations have also been developed around the basic GTAW method. Such variations, which are extensively described in reference [9], include, for example: Activated TIG (A-TIG), a method based on applying a surface-active flux coating to the surface of a workpiece prior welding, a process variation based on keyhole welding, i.e., K-TIG method, which uses very high welding currents, and a pulse welding method in which the welding current is varied between two current values. In the pulse welding method, the current varies between the basic current, i.e., the background current, and the pulse current, i.e., the peak current, at a predetermined and repetitive pulse frequency. During the pulse current phase, a melt pool and a weld penetration are formed. During the base current phase, the weld pool cools and solidifies into the weld metal. By adjusting the pulse parameters, heat input and melt control can be affected. The regulation of heat input has an effect on, among other things, the shape, penetration and microstructure of the weld and, consequently, on the mechanical and chemical (corrosion resistance) properties of the joint. The effect of GTAW pulse parameters and their use are described in detail, for example, in references [10-16]. By adjusting the heat input with correctly set pulse parameters, it also allows control of the melt pool and enables welding in different welding positions, such as vertical and overhead position [17].

The choice of shielding gas in GTAW is also an essential parameter that can be used, for example, to influence the achievable penetration of the weld joint. In references [18-20], the researchers have studied the effect of the shielding gas and gas mixture composition on the properties of stainless steel welds produced with GTAW. The common understanding of the above studies has been that especially the addition of hydrogen to the argon base gas results in an improvement in the penetration of the weld. In particular, a 1-2% hydrogen addition in the argon base gas would appear to be the optimal amount at which, in addition to weld penetration, the quality and mechanical properties of the weld are at their best.

The versatility of GTAW enables the process to be applied both in manual and mechanized or automatic welding operations. In industrial welding applications, it is used as an automated process for example in orbital welding of nuclear power plant components and tube-to-tube sheet welding in the manufacture of heat exchangers [21,22]. One recent area of research and manufacturing has been the fabrication and assembly of components for an experimental fusion power plant utilizing the GTAW process [23-25]. In addition, during future maintenance outages of the aforementioned fusion power plant, it will be necessary to re-weld certain joints in the service opening structures. The re-welding mentioned in the maintenance work must be performed as automated remote welding in order to avoid the radioactive radiation exposure of workers.

The aim of this study is to investigate the applicability of GTAW process for the robotized position welding of an edge joint configuration made of austenitic stainless steel sheets. The main objective was to determine the welding parameters suitable for position welding by means of an optimized pulse welding method and shielding gas selection. In connection with the optimization of the welding parameters, a penetration of at least 2.6 mm was required for the completed weld joint. Another objective was to form an understanding of how well a used welding process withstands the inaccuracy associated with welding torch alignment relative to a weld joint.

Materials and methods

Test specimens used in welding experiments were made from ordinary AISI 316L austenitic stainless steel sheets of 2 mm thickness. The joint type used in the experiments was an edge joint. The test specimens were laser cut from the sheets. The test specimens were both rectangular shaped 450 mm x 100 mm (length x width, respectively) in size and curved corner-shape specimens with vertical and horizontal portions. In Fig. 1a it can be seen the geometries of test specimens along with their main dimensions. Fig. 1b shows the edge joint configuration used and the principle how joint penetration was determined from the cross-section of welded joints.

A standard ESAB Aristo welding machine with gas tungsten arc welding equipment was used in the experiments. Welded test specimens were fastened into a purposely made welding jig which stands on a vertical column and has two multiple screw tightened clamping jaw plates and incorporated pivot axle which abled rotation and locking of test specimens into the orientation which represents required welding positions. An articulated arm robot was applied to carry out the arc torch movements and trajectories of required welding positions. The configuration of above-mentioned welding set-up can be seen in Fig 2.

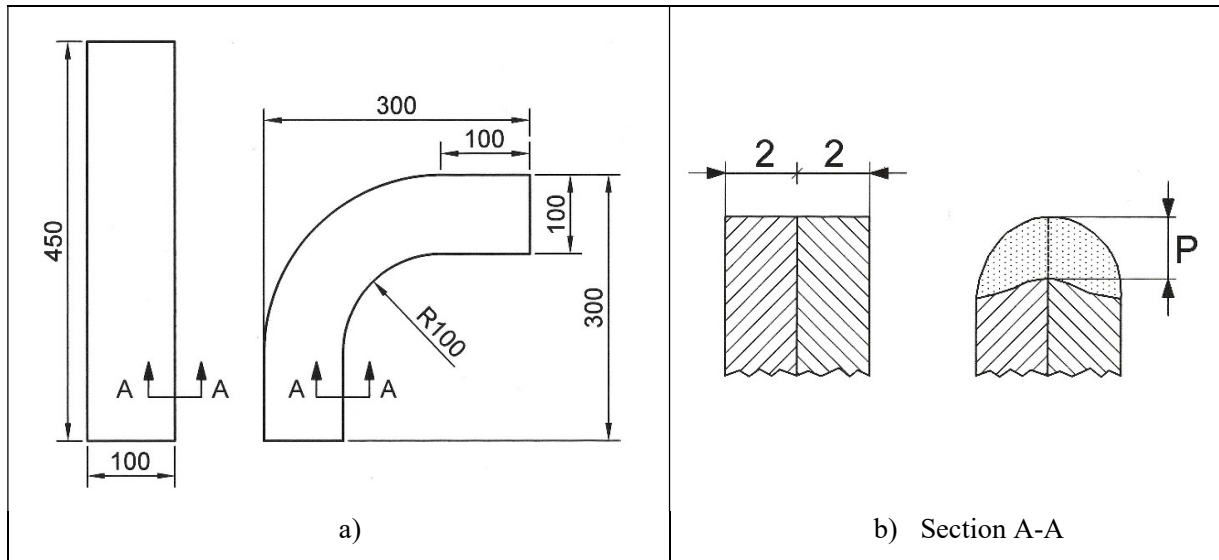


Fig. 1. a) Geometries and main dimensions of test specimens fabricated from 2 mm thick AISI 316L sheets. b) Section A-A from fig. a) showing edge joint configuration used and a schematic of principle how joint penetration (marked with P in fig. b) is determined from the cross-section of welded joint. Dimensions are in millimeters.

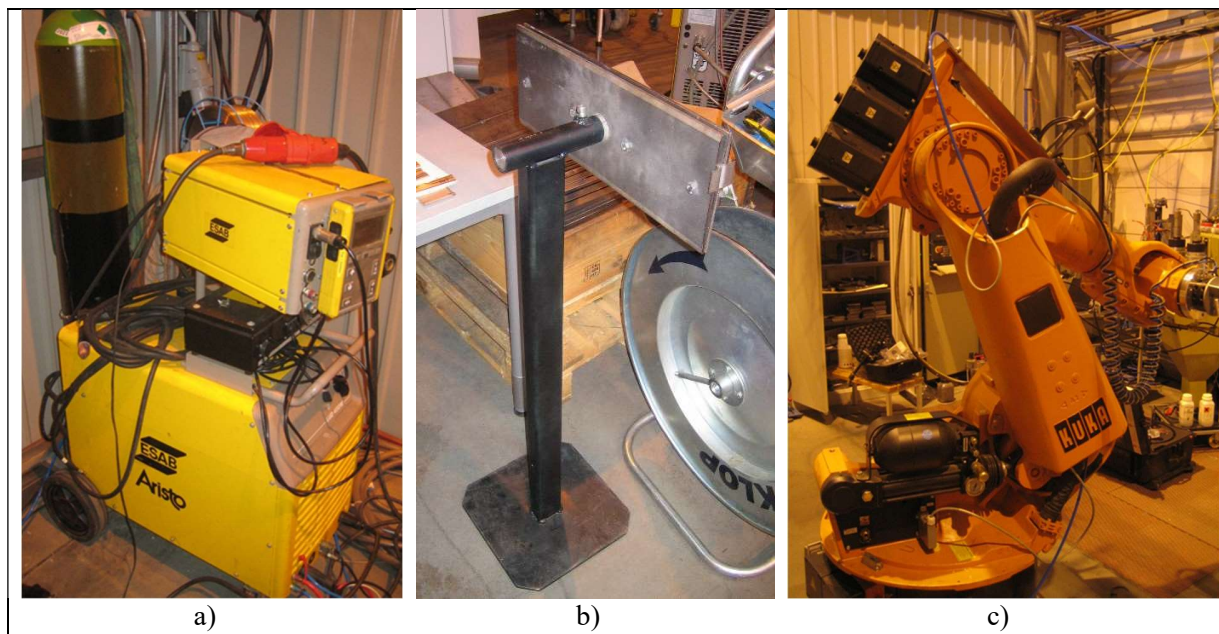


Fig. 2. Welding set-up used in the experiments: a) Gas tungsten arc welding machine, b) welding jig with rotatable fixture, c) articulated arm robot for execution of welding movements.

Experimental procedure

Experimental work was divided in several phases. In the phase 1, preliminary welding tests with using a pure argon shielding gas were carried out to determine an adequate window for the combination of GTA pulse parameters and applicable welding speed range which would produce best achievable weld joint penetration with good melt pool control in position welding. Details and summary of welding parameters used in phase 1 are presented in Table 1.

Table 1. Welding parameters used in the experiments of phase 1.

Constant parameters	Values
Current / polarity	Direct current / straight polarity (electrode negative)
Electrode type and dimensions	2%-thoriated tungsten, diameter Ø 2.4 mm, vertex angle 90°, truncated tip Ø 0.5 mm
Torch angle	Parallel to joint, travelling angle perpendicular to joint
Electrode stand-off distance	2 mm
Shielding gas and flow rate	Argon, 14 l/min
Variable parameters	Values / range
Pulse current	174 – 188 A
Background current	30 – 34 A
Pulse time	0.05 – 0.10 s
Background time	0.1 – 0.25 s
Welding speed	200 – 300 mm/min
Welding positions	Flat (PA), vertical-up (PF) vertical-down (PG) and overhead (PE)

In the phase 2, welding experiments with three different Argon based gas mixture compositions were carried out to find out whether there would be any benefit when aiming deeper weld joint penetration compared to the results when regular argon shielding gas was used. Details and summary of welding parameters used in phase 2 are presented in Table 2.

Table 2. Welding parameters used in the experiments of phase 2.

Constant parameters	Values
Current / polarity	Direct current / straight polarity (electrode negative)
Electrode type and dimensions	2%-thoriated tungsten, diameter Ø 2.4 mm, vertex angle 90°, truncated tip Ø 0.5 mm
Torch angle	Parallel to joint, travelling angle perpendicular to joint
Electrode stand-off distance	2 mm
Shielding gas flow rate	14 l/min
Pulse current	180 A
Background current	32 A
Pulse time	0.1 s
Background time	0.22 s
Welding speed	200 mm/min
Welding position	Vertical up (PF)
Variable parameters	Values / range
Shielding gas variants	Ar+2% CO ₂ , Ar+2% CO ₂ + 30% He, Ar+2%H ₂ ,

In the phase 3, the most optimal welding parameter combination determined during the phase 1 and 2 was put to further test, where curved corner-shape specimens with vertical and horizontal portions were welded comprising a combination of flat (PA), vertical-up (PF) and overhead (PE) welding positions. Details and summary of welding parameters used in phase 3 are presented in Table 3.

Table 3. Welding parameters used in the experiments of phase 3.

Constant parameters	Values
Current / polarity	Direct current / straight polarity (electrode negative)
Electrode type and dimensions	2%-thoriated tungsten, diameter Ø 2.4 mm, vertex angle 90°, truncated tip Ø 0.5 mm
Torch angle	Parallel to joint, travelling angle perpendicular to joint
Electrode stand-off distance	2 mm
Shielding gas and flow rate	Ar+2%H ₂ , 14 l/min
Pulse current	180 A
Background current	32 A
Pulse time	0.1 s
Background time	0.22 s
Variable parameters	Values / range
Welding speed	200 mm/min in PA and PE position, 220 mm/min in PF position
Welding positions	flat (PA), vertical-up (PF) and overhead (PE)

In above mentioned experiments of phase 3, the welding of test weld RA started at vertical-up position and welding continued up along the inner curve with 100 mm radius and then shifted into overhead position where it has finally the weld finishing location. As regards to another test weld RB, the welding started at flat position (PA) and welding continued up along the inner curve with 100 mm radius and then shifted into vertical-up (PF) position where was finally the welding finishing location. The schematic presentation showing the used test samples RA and RB, together with the used welding path are shown in Fig 3. In addition, a smooth weld starting and finishing procedure consisting controlled welding energy ramping (increasing/decreasing welding arc energy within certain time frame) was determined in phase 3 and the outcome are presented in the result section.

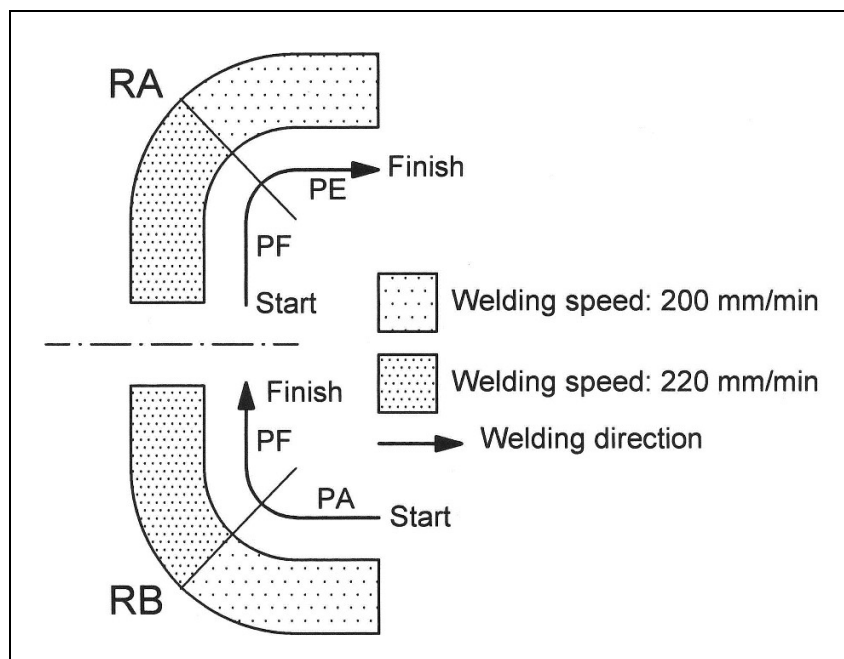


Fig. 3. Schematic presentation showing curved corner-shape test specimens along with their welding paths used in multiple welding position experiments carried out in phase 3. Used positions in test sample RA: Vertical-up (PF) → transition positions between PF and PE at the corner → overhead (PE) position. In test sample RB: Flat (PA) → transition positions between PA and PF at the corner → vertical-up (PF) position. Black arrowed lines show welding directions.

Finally, in the phase 4, further set of welding experiments were made to find out how robust used welding procedure is against to different variance of electrode distance and alignment respect to joint centre line. Details and summary of welding parameters used in the phase 4 are presented in Table 4.

Table 4. Welding parameters used in the experiments of phase 4.

Constant parameters	Values
Current / polarity	Direct current / straight polarity (electrode negative)
Electrode type and dimensions	2%-thoriated tungsten, diameter Ø 2.4 mm, vertex angle 90°, truncated tip Ø 0.5 mm
Shielding gas and flow rate	Ar+2%H ₂ , 14 l/min
Pulse current	180 A
Background current	32 A
Pulse time	0.1 s
Background time	0.22 s
Variable parameters	Values / range
Torch angle	Parallel to joint = tilt angle 0°, tilt angle 5°, tilt angle 10°
Electrode stand-off distance	1.5 mm, 2 mm, 2.5 mm
Vertical misalignment of joint sheet edge	0.5 mm, 0.7 mm
Welding speed	200 mm/min in PA and PE position, 220 mm/min in PF position
Welding positions	flat (PA), vertical-up (PF) and overhead (PE)

The test matrix carried out in the phase 4 for testing robustness of welding process against different misalignment errors (both arc torch orientation and joint configuration related) is presented in Table 5. In Fig. 4 (a-c) it also is schematically illustrated the tested misalignment error variants.

Table 5. Test matrix carried out in the phase 4 to test tolerance of welding process against different misalignment errors.

Test piece ID	Welding position	Electrode stand-off distance [mm]	Torch tilt angle [°]	Electrode horizontal offset [mm]
KA1	PF	1.5	0	0
KA2	PF	2.5	0	0
KA3	PF	2	5	0
KA4	PF	2	10	0
KA5	PA	1.5	0	0
KA6	PA	2.5	0	0
KA7	PA	2	5	0
KA8	PA	2	10	0
KA9	PE	2.5	0	0
KA10	PE	1.5	0	0
KA11	PE	2	5	0
KA12	PE	2	10	0
KA13	PA	2	0	0.5
KA14	PA	2	5	0.5
KA15	PF	2	5	0.5
KA16*	PF	2	5	0.7
KA17*	PF	2.5	5	0.5

* Note: Vertical sheet misalignment of joint assembly was set to 0.5 mm.

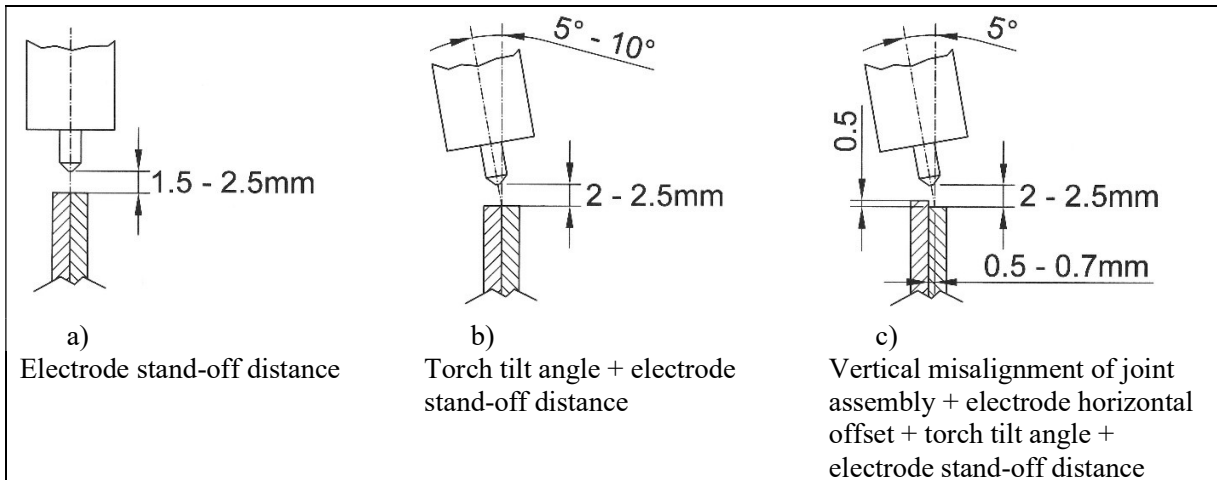


Fig. 4. Illustration of variable parameters which were applied to test robustness of welding process against different misalignment errors.

Assessment of welding performance were made using visual inspection and based on produced weld penetration profiles of test welds which were determined from the selection of cross-sectional macro graphs.

Results and discussion

Phase 1 – Welding optimization trials using pulsed GTA parameters for position welding

At first, a correct relationship between pulse parameters and welding speed was established. The ratio between background and pulse current along with background and pulse time was aimed to be fit with maximum usable welding speed. Studied pulse parameters were as follows: Pulse current (I_p), background current (I_b), pulse time (t_p), background time (t_b), see Fig.5.

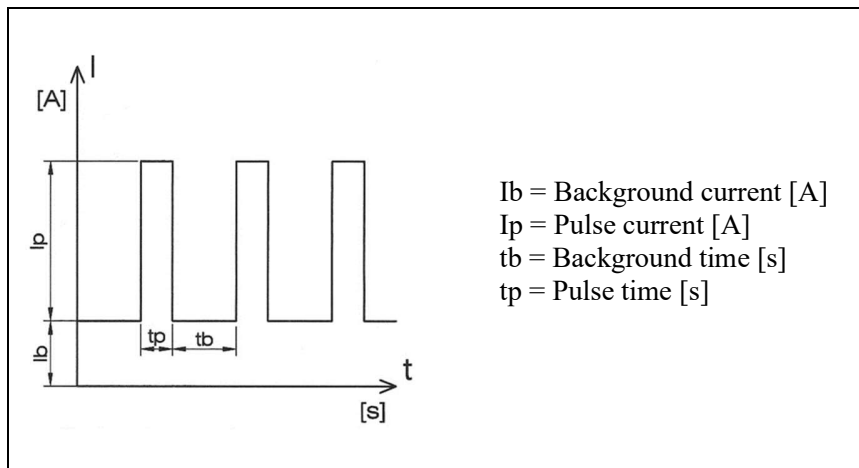


Fig. 5. Gas tungsten arc (GTA) pulse parameters.

During the preliminary welding experiments it was perceived that a direct current (DC) welding with a pulsed mode can offer means to control melt pool (size, shape and penetration) and to cope with the effect of gravity in especially in vertical welding position: Weld penetration is generated during the pulse current and its pulse time, whereas during the background time current has to be fitted low enough in order to secure that the volume of weld pool do not grow too large and has proper time to solidify.

It was experienced that there could be found parameter window where a very delicate balance between down-ward melt flow and weld solidification applies. If that threshold is exceeded, it will result disturbed welding process and weld sagging. In Fig. 6, it can be seen an example of weld appearance where severe weld sagging has appeared in a vertical position welding experiment due to unsuitable welding parameters. As regards to weld joint penetration, in flat welding position (PA) welding current could be raised higher without the risk of weld sagging and penetration values over 2 mm were measured from the studied weld cross-sections. Nevertheless, in other welding positions (PF, PG and PE) a lower-level current needed to be applied to secure that melt pool do not grow too large causing tendency to weld sagging. The imbalanced down-ward melt flow due to effect of gravitation was the most restrictive factor for not achieving a higher level of joint penetration with successful welding outcome in vertical position, especially in vertical-down welding position.

In general, based on the results of phase 1, the following pulse parameter and welding speed window could be drawn.

- Pulse current (I_p) / background current (I_b) \rightarrow ratio of (I_p) / (I_b) $\sim 5 \dots 6$
- Pulse time (t_p) / background time (t_b) \rightarrow ratio of (t_p) / (t_b) $\sim 0.3 \dots 0.5$
- Welding speed range: 200...300 mm/min

The best pulse parameter and welding speed combination which equally could be applied to all tested welding positions was determined to be as follows: Pulse current (I_p) = 180 A, background current (I_b) = 32 A, Pulse time (t_p) = 0.1 s and background time (t_b) = 0.22 s which corresponds around 3 Hz pulse frequency. Welding speed in PA and PE position = 200 mm/min and in PF and PG position = 220 mm/min.

The macro graphs showing the weld-cross-sections with penetration profiles are presented in Fig. 7. When weld penetration profiles are examined in general, it can be noticed that when a full argon shielding gas composition is used, the base metal has vertically melted further at the surface region of the sheets than when compared to the center area along the weld joint line. It appears that the welding energy density of arc flux has not been sufficient to melt the base metal evenly throughout the joint cross-section, leaving unfused base metal peninsula at center area of joint line. Above was the reason that achieved weld joint penetration values were quite moderate compared to initial aim. In flat position (PA), vertical-up (PF) and overhead (PE) position achieved joint penetration was between 1.7 and 1.6 mm. In vertical-down (PG) position, however, the joint penetration remained at a maximum of 1.4 mm level. Moreover, PG welding position was most sensitive to imbalanced down-ward melt flow, which in turn caused detrimental weld sagging. That is why in subsequent test phases it was decided to concentrate on PA, PF and PE positions.



Fig. 6. Example showing weld sagging tendency occurring in vertical welding position.

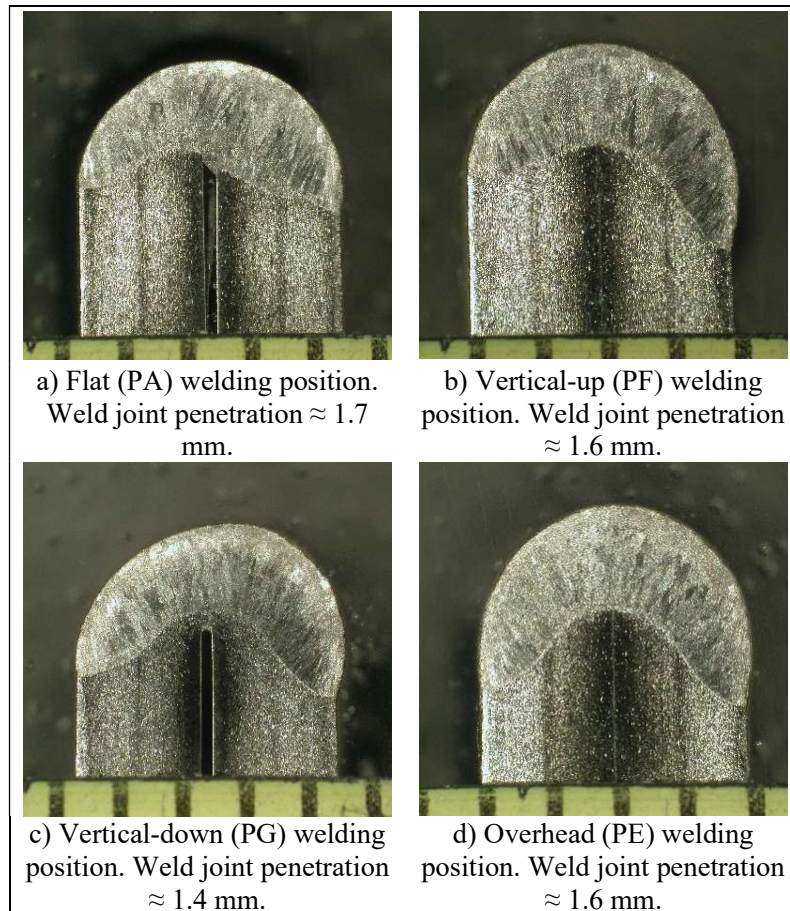


Fig 7. Edge joint weld cross-sections (a-d) produced with optimized welding parameters using a plain argon shielding gas composition in experiments of phase 1. In the scale strip, one interval corresponds to 1 mm.

Phase 2 – Effect of shielding gas composition variants on weld joint penetration

During the experiments carried out in phase 1, it became evident that with using a full argon shielding gas (Mison Ar) composition, the pre-set aim of weld joint penetration of 2.6 mm in all welding positions cannot be reached. Typical penetration values achieved with using plain argon shielding lied below 2 mm. A most challenging melt pool controllability was experienced in vertical-down (PG) position welding and the maximum penetration which could be accomplished without a weld sagging was limited to the value of 1.4 mm. That is why PG position was omitted in the subsequent test phases.

In phase 2 it was decided to try three different commercially available argon based gas mixtures (Table 2) and investigate if there will be any help to generate more weld joint penetration compared to plain argon shielding. The welding position used in tests of phase 2 was solely vertical-up (PF) position because it was experienced in phase 1 that it was the second most challenging position what comes to weld pool control after vertical-down (PG) position.

As regards to investigating the effect of shielding gas composition variants on weld joint penetration, the first approach was to use a mixture containing argon as a base gas and 2% CO₂–addition (Mison2) in it. The investigations indicates that this allows a bit higher pulse current value to be used, which gave a better weld penetration leading to the penetration value of approx. 2.3 mm (Fig. 7a). The following alternative gas was a mixture containing argon as a base gas and 30% helium and 2% CO₂–addition (Mison2He) in it. Using Mison2He shielding gas also a bit higher pulse current could be used. Also, a bit higher welding speed compared to MisonAr and Mison2 could be applied. Nevertheless, the weld penetration with Mison2

and Mison 2He) stayed slightly less than 2.5 mm, with typical values being $\sim 2.3 \dots 2.4$ mm (Fig. 8a and 8b). Finally, the best penetration result was achieved when shielding gas with 2% hydrogen addition in argon was used (MisonH₂). Using MisonH₂ shielding gas, the penetration requirement of 2.6 mm could be reached when typical values were 2.6...3 mm (Figs. 8c and 8d). Moreover, if the shapes of weld cross-sections (Figs. 8c and 8d) are compared to ones (Fig. 7) produced using plain argon shielding gas (MisonAr), MisonH₂-gas gave more evenly distributed penetration profile across the joint area. It can also be observed from weld cross-sections of Fig. 8c and 8d, that there is less joint penetration in the weld cross-section presented in Fig. 8c than in Fig. 8d, although they were welded using the same parameters. The cross-section of the weld in Fig. 8c has been tilted somewhat to the right-hand side, which diminishes the penetration measured along the joint line. The reason for tilting was associated with welding torch misalignment (angular and perpendicular) respect to the joint centre line. Because an edge joint does not provide any inherent support surface on sideways, the melt could easily flow on sideways, and it remains tilted upon the solidification. Welding experiments showed the signs that the pre-set penetration requirement of 2.6 mm was pushing weld pool control and stability near the threshold limit, where “weld tilting” phenomena could be susceptible to angular and perpendicular misalignment of welding torch.

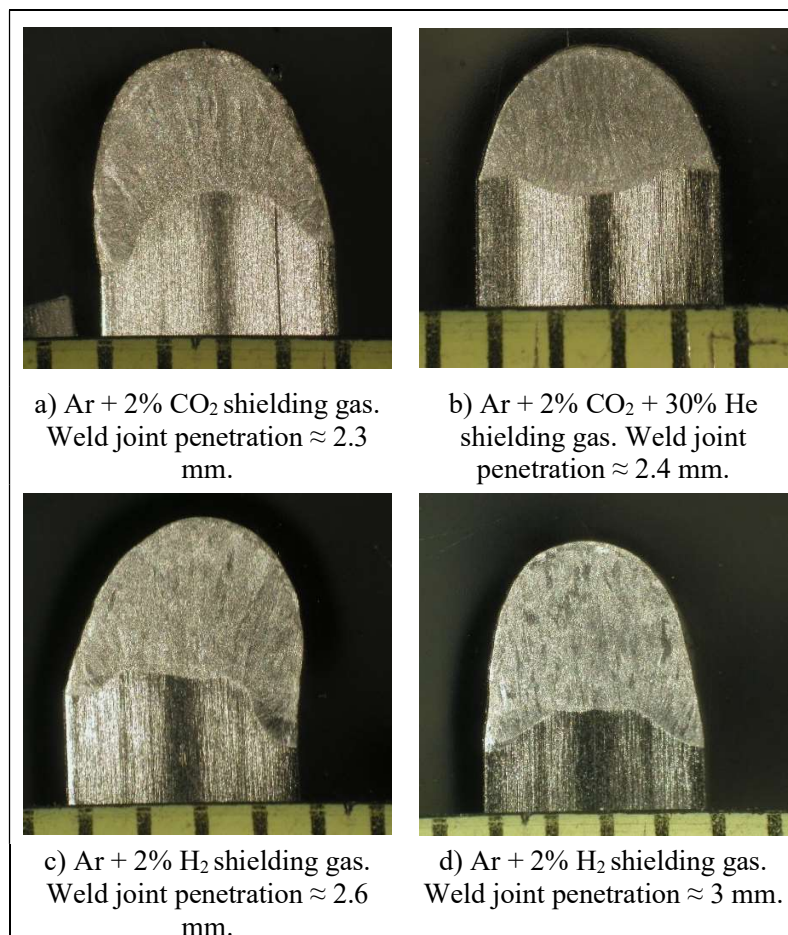


Fig 8. Edge joint weld cross-sections produced in vertical-up (PF) position and using optimized welding parameters and with different shield gas composition variants tested in the experiments of phase 2. In the scale strip, one interval corresponds to 1 mm.

Phase 3 – Welding experiments with curved L-shape specimens in multiple positions and welding start/finish procedure

In order to put the optimized welding parameters (e.g. the pulse parameters, Ar+2% H_2 shielding gas, etc.) established in the phase 1 and 2 to the further test, curved test samples were applied next. The purpose was to check a position welding capability and at the same to imitate the welding of corner/curved locations in circumferential joints.

Figs. 9a and 9b represent welded test specimen RA and RB and show the locations where the weld cross-sections have been cut out for metallographic examination. As the weld cross-sections from Fig. 10 are examined, the penetration profiles of the sample RA test weld are quite symmetrical and the penetration requirement (2.6 mm) in the direction of the joint was met, while the penetration values were 2.8 to 3.2 mm. What comes to the weld penetration profiles of specimen RB, it can be judged from the Fig. 11 that weld profiles are tilted ca. 30...40 degree, leading an insufficient penetration (from 2 to 2.5 mm) along the joint direction. Mentioned tilting of the welding profile is due to the misplacement of the welding torch, which causes the molten pool to move sideways relative to the weld joint. Distortions occurred during the welding is anticipated to be a major reason for torch misalignment because the torch orientation and the used welding path was carefully determined and taught to robot prior the welding. The repeatability accuracy of modern industrial high-accuracy articulated arm robots can even be up to +/- 0.05 mm, which guarantees precise welding movements. Therefore, in applications with a lot to be welded, i.e. long welds, due to welding distortions, it is recommended to use a seam tracking system integrated in the welding head attached to the wrist of the robot. The seam tracking system help the progress of welding by making the necessary position corrections to the tool center point (TCP), i.e. the tip of the electrode, by compensating for the position error caused by the welding distortions relative to the original position information.

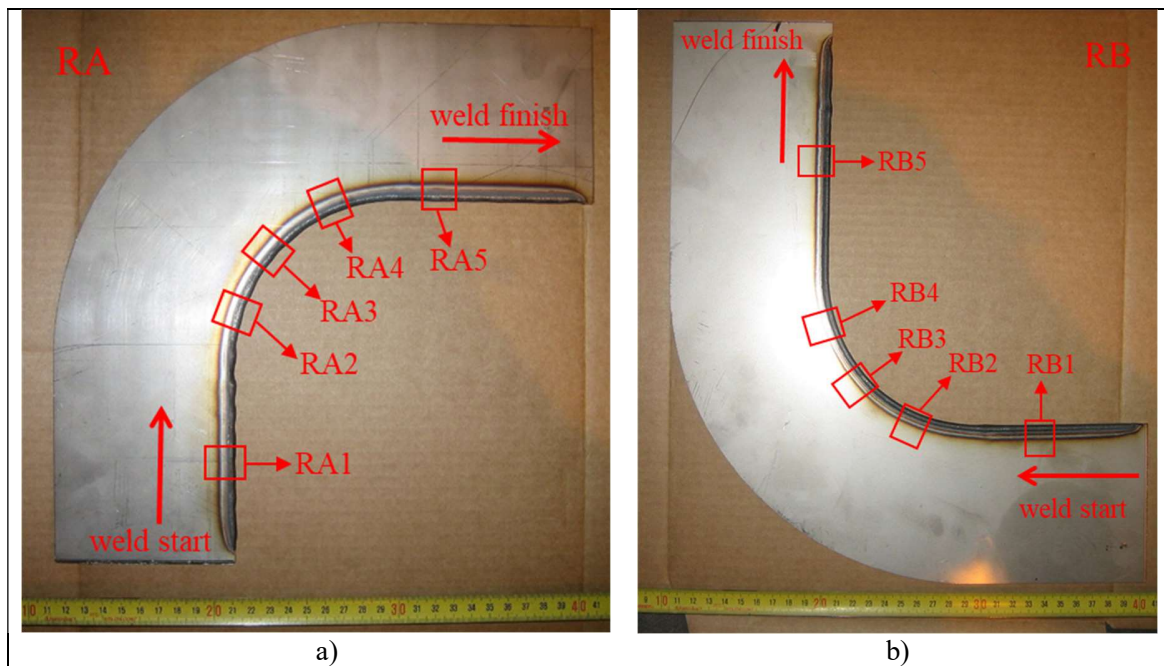


Fig 9. Edge joint weld produced in test specimen RA (a) and RB (b). The red boxes indicate the locations from which the macro cross-sectional samples of the weld were cut.

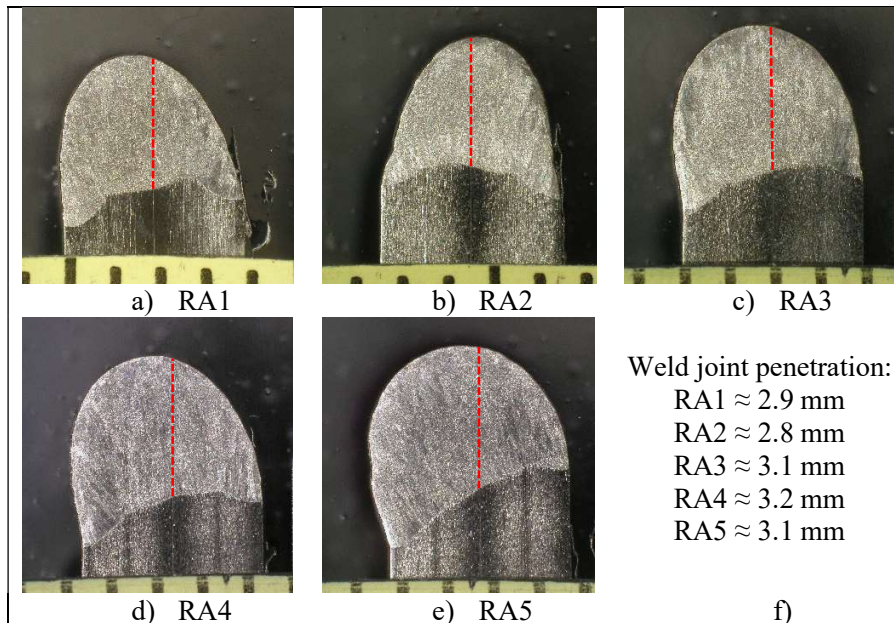


Fig 10. Weld cross-sections from the welded edge joint of test specimen RA. Red dashed line indicates the location from which the weld joint penetration is measured. In the scale strip, one interval corresponds to 1 mm.

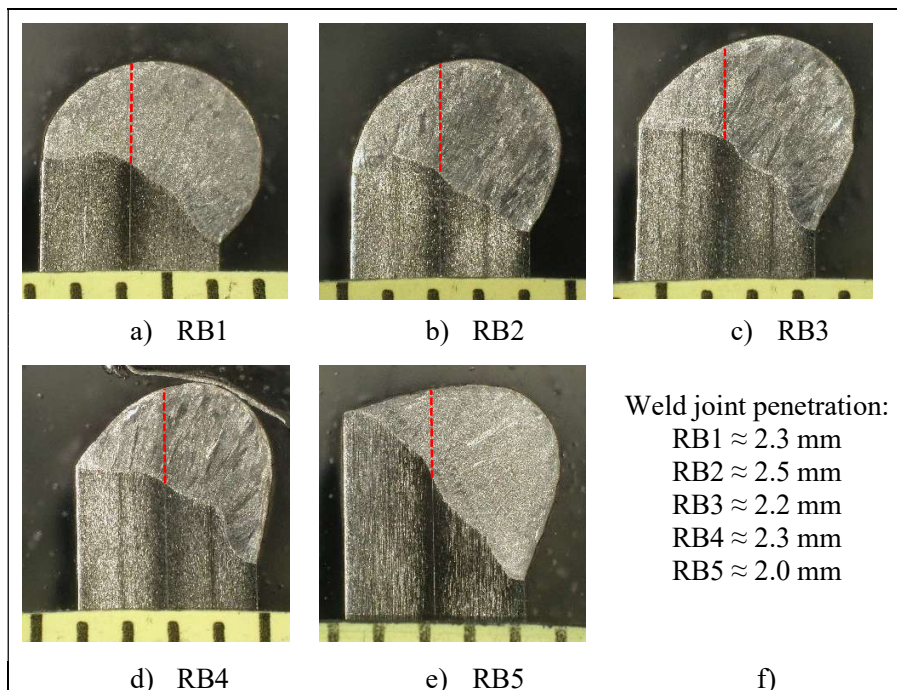


Fig 11. Weld cross-sections from the welded edge joint of test specimen RB. Red dashed line indicates the location from which the weld joint penetration is measured. In the scale strip, one interval corresponds to 1 mm.

If welding of circumferential joints is aimed, the welding with using PA, PF and PE positions will require at least two starting and two finishing locations to cover a full joint perimeter. It was foreseen that welding of such a circumferential joint for inner edge would be produced e.g., having a first half of weld path starting at 6 o'clock with PA position, then proceeding clockwise and ending in PE position at a 12 o'clock. The

second half of weld path would be produced as a reversed, starting at 6 o'clock with PA position, then proceeding counter-clockwise and ending in PE position at a 12 o'clock. Above-described welding path arrangement scenario are schematically presented in Fig. 12.

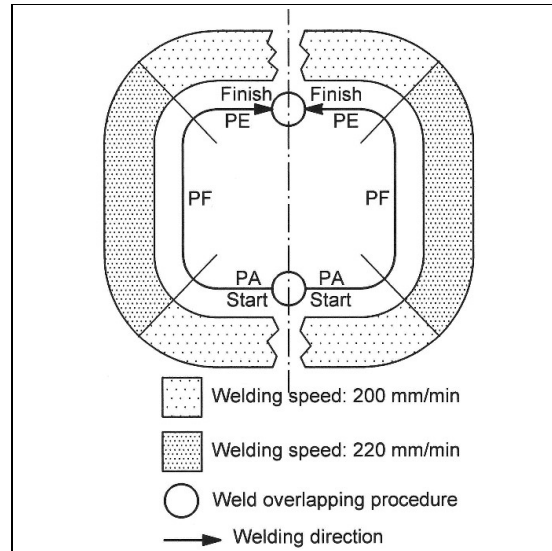


Fig 12. Schematic presentation of welding sequence arrangements that may be considered applicable to position welding of the inner edge of a circumferential joint.

A well-controlled start and finishing manoeuvre should be applied to achieve proper transition between above mentioned start and finish points. To address above issue, a set of test trial was conducted in which welding energy was ramped respect to used arc interaction time. The following procedure was used: At the start, welding energy was linearly increased from zero to pre-set full power within the time frame of 3 seconds. At the finish point, welding sequence was proceeded just over the start point (overlapping) and then welding energy was linearly reduced from full power to zero within the time frame of 3 seconds. As using the welding speed of 200 mm/min, the length of transition zone during the welding energy ramping is approximately 10 mm. Both the start (in the PA position) and the finish (in the PE position) procedure are partially overlapped on the pre-existing weld. Figs. 13a and 13b show the longitudinal weld cross-sections from the welding start and welding finish test welds, respectively. The triggering locations where the welding start and finish procedures are turned on are pointed out with white dashed lines. The longitudinal cross-sections reveal a smooth linear transition where weld penetration is gradually increased and decreased in overlapping locations of start and finish respectively.

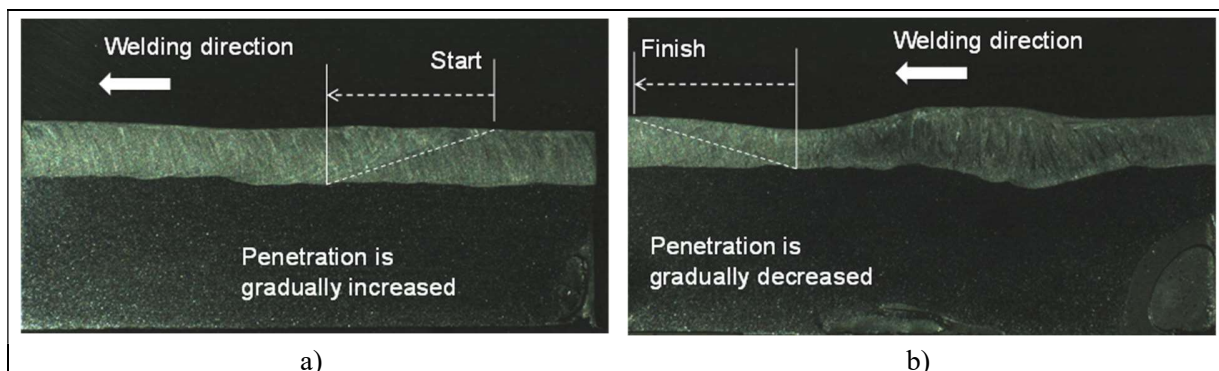


Fig 13. Longitudinal weld cross-sections showing a smooth linear transition zone of weld penetration in overlapping locations of start (a) and finish (b) procedure.

Phase 4 – Assessment of the effect of electrode misalignments and joint inaccuracy on weld penetration and overall process performance

In previous experiments, it was found that the correct orientation and position of the arc torch relative to the centerline of the weld joint is important to achieve proper control of the melt pool and penetration of the joint. Therefore, in phase 4, additional welding experiments were performed to evaluate how tolerant the welding process is to the variation of the stand-off distance and alignment of the electrode as well as to the vertical alignment error of the weld joint. The used constant welding parameters were the same as optimized in phase 1 and 2. The matrix showing the tested combinations of variables is presented in Table 5.

The first six trials (test weld KA1, KA2, KA5, KA6, KA9 and KA10) started using vertical up (PF, test weld KA1 and KA2), flat (PA, test weld KA5 and KA6) and overhead (PE, test weld KA10 and KA9) welding positions and ± 0.5 mm variation from the nominal/optimal electrode stand-off distance of 2 mm. The weld cross-sections of those test welds are shown in Figs. 14 a-f. When studying the weld penetration profiles, following weld joint penetrations were measured when electrode stand-off distance value of 1.5 mm was used: KA1 ≈ 3.3 mm, KA5 ≈ 2.5 mm, KA10 ≈ 2.7 mm. When the used electrode stand-off distance value was 2.5 mm, the corresponding penetration values were: KA2 ≈ 3.7 mm, KA6 ≈ 2.7 mm and KA9 ≈ 3.0 mm. It was noticed during the welding experiments, that the electrode distance of 1.5mm was a bit too less because the electrode was once about to stick into the solidifying melt pool. Moreover, the used 1.5 mm electrode distance tends to produce a bit smaller penetration value. When the electrode distance is increased by 0.5 mm from a nominal value of 2.0 mm to a value of 2.5 mm, the penetration profiles appeared to be formed properly. Thus, it can be assessed that the electrode stand-off distance should be kept in the 2 - 2.5 mm range.

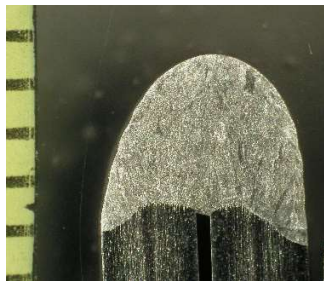
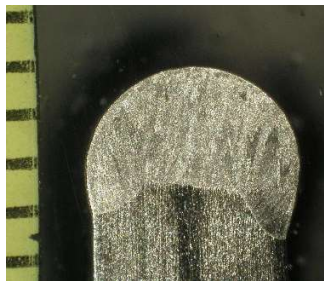
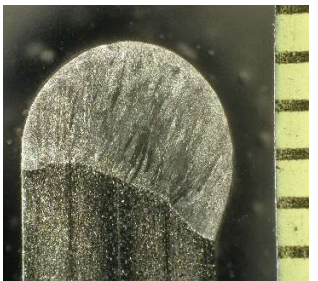
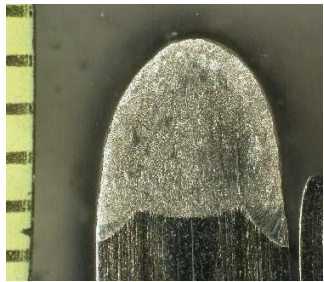
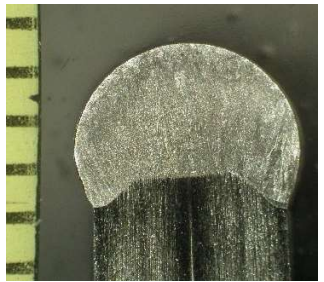
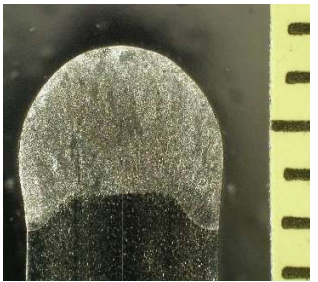
		Welding position		
		PF	PA	PE
Electrode stand-off distance [mm]	1.5			
		a) Test weld KA1	b) Test weld KA5	c) Test weld KA10
	2.5			
		d) Test weld KA2	e) Test weld KA6	f) Test weld KA9

Fig 14. Weld cross-sections from the experiments testing the effect of variable (1.5 mm and 2.5 mm) electrode stand-off distances on welding performance in PA, PF and PE positions. In the scale strip, one interval corresponds to 1 mm.

The following six trials (test weld KA3, KA7, KA11, KA4, KA8 and KA12) consisted of vertical up (PF, test weld KA3 and KA4), flat (PA, test weld KA7 and KA8) and overhead (PE, test weld KA11 and KA12) welding positions and 5- and 10-degree tilting of torch respect to joint. Electrode stand-off distance was nominal 2 mm. The weld cross-sections of those test welds are shown in Figs. 15 a-f. When studying the weld penetration profiles, following weld joint penetrations were measured: KA3 \approx 2.8 mm, KA7 \approx 2.8 mm, KA11 \approx 3.2 mm, KA4 \approx 2.5 mm, KA8 \approx 2.3 mm and KA12 \approx 3.1 mm. It can be concluded from the cross-sections of Figure 15 a-c that the welding process can tolerate a 5-degree torch tilt configuration that still produces required weld joint penetration. However, looking at the cross-sections d-f in Figure 15, as the tilt of the torch increases to 10 degrees, it begins to have a greater effect on the welding profile by reducing the penetration of the joint. This can be seen in the Figs. 15d and 15e, in which test weld KA4 and KA8 have tilted welding profiles with reduced weld joint penetration. Based on the above observations, it can be assessed that the tilt angle of the welding torch must not exceed 5 degrees from the direction of the vertical axis of the joint.

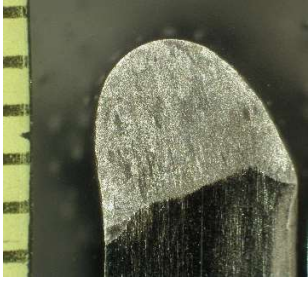

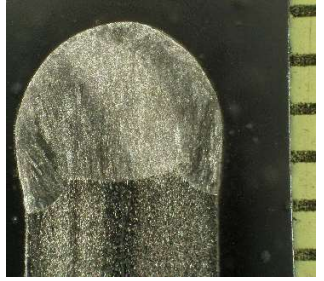
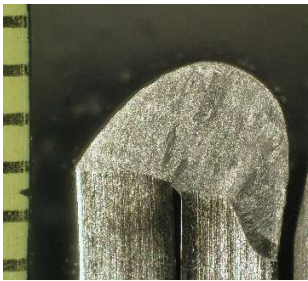

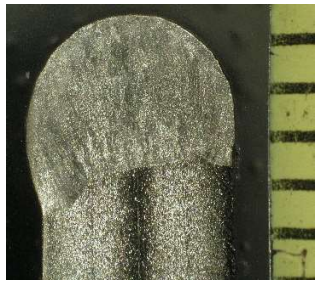
		Welding position		
		PF	PA	PE
Torch tilt angle [°]	5			
		a) Test weld KA3	b) Test weld KA7	c) Test weld KA11
	10			
		d) Test weld KA4	e) Test weld KA8	f) Test weld KA12

Fig 15. Weld cross-sections from the experiments testing the effect of variable (5-degree and 10-degree) torch tilt angle on welding performance in PA, PF and PE positions. In the scale strip, one interval corresponds to 1 mm.

The third set of tests consisted of five test welds (KA13, KA14, KA15, KA16, KA17). The purpose was to test the ability of the welding process to withstand the combined effect of the vertical, horizontal and angular positioning error of the electrode and the vertical misalignment of the joint assembly in the PF and PA welding positions. The macro cross-sections of above welds are presented in Fig. 16.


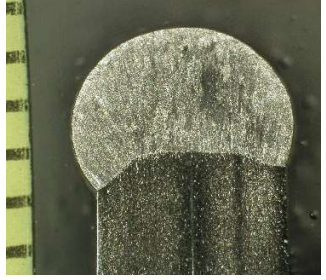



		Combinations of positioning variables		
Welding position	PA	Electrode position: <ul style="list-style-type: none"> ▪ HOS = 0.5 mm ▪ SOD = 2 mm ▪ TA = zero ▪ VMJ = zero  <p>a) Test weld KA13</p>	Electrode position: <ul style="list-style-type: none"> ▪ HOS = 0.5 mm ▪ SOD = 2 mm ▪ TA = 5° ▪ VMJ = zero  <p>b) Test weld KA14</p>	Abbreviations: <ul style="list-style-type: none"> ▪ HOS = Horizontal off-set ▪ SOD = Stand-off distance ▪ TA = Tilt angle ▪ VMJ = Vertical misalignment of the joint assembly
	PF	Electrode position: <ul style="list-style-type: none"> ▪ HOS = 0.5 mm ▪ SOD = 2 mm ▪ TA = 5° ▪ VMJ = zero  <p>c) Test weld KA15</p>	Electrode position and joint: <ul style="list-style-type: none"> ▪ HOS = 0.7 mm ▪ SOD = 2 mm ▪ TA = 5° ▪ VMJ = 0.5 mm  <p>d) Test weld KA16</p>	Electrode position and joint: <ul style="list-style-type: none"> ▪ HOS = 0.5 mm ▪ SOD = 2.5 mm ▪ TA = 5° ▪ VMJ = 0.5 mm  <p>e) Test weld KA17</p>

Fig 16. Weld cross-sections from the experiments testing the effect of combined misalignment factors on welding performance in PA and PF positions. In the scale strip, one interval corresponds to 1 mm.

When the weld joint penetration profiles from Figs. 16a-e are studied, it can be concluded that welding process can tolerate different combined misalignment configurations used in the third set of trials. The following detailed findings can be highlighted. The weld joint penetrations measured from the cross-sections were all at the acceptable level (2.6 mm or higher): KA13 \approx 2.7 mm, KA14 \approx 2.6 mm, KA15 \approx 3.1 mm, KA16 \approx 3.1 mm and KA17 \approx 3.4 mm. The allowable horizontal off-set of the electrode alignment appeared to be tolerable up to 0.7 mm from the centerline of the joint, but it is recommended that the value not exceed 0.5 mm. The vertical misalignment of joint assembly used in test welds KA16 and KA17 was 0.5 mm. Judging from the welding cross-sections (Figs. 16d and 16e), it appears that the combined offset variance (HOS = 0.5-0.7 mm + VMJ = 0.5 mm) can be welded acceptably. With respect to torch alignment requirements, the results of the second and third test series confirmed that an important factor is to ensure that the torch angle is aligned as accurately as possible along the weld joint so as not to exceed a 5-degree tilt value.

Conclusions

The work presented in this study included both parameter optimization and evaluation of welding performance in the gas tungsten arc welding process in robotic position welding of an austenitic stainless steel edge joint. In connection with the optimization of the welding parameters, a penetration of at least 2.6 mm was required for the completed weld joint. The study conducted several welding experiments to evaluate the overall performance of welding, in particular how the welding process withstands variations that occur in the stand-off distance and alignment of the electrode, as well as in the vertical misalignment of the weld joint. The following conclusions can be drawn from the results of the research carried out in this work:

A pulsed mode direct current GTAW with a relatively low 3 Hz cycle frequency used together with a shielding gas composition containing 2 % hydrogen in argon base gas was found to be the key factors to achieve penetration requirement of 2.6 mm in edge joint welds. Used optimal pulse parameters can offer means to control melt pool (size, shape and penetration) and to cope with the effect of gravity in especially in vertical welding position. Weld penetration is generated during the pulse current and its pulse time, whereas during the background time current has to be fitted low enough in order to secure that the volume of weld pool do not grow too large and has proper time to solidify without a weld sagging defect.

Welding tests showed that the required 2.6 mm weld joint penetration requirement can be achieved in flat (PA), vertical-up (PF) and overhead (PE) positions. In the vertical-down position (PG), the effect of gravity on the melt pool limited the amount of penetration that could be achieved, which was less than 2 mm. Therefore, to avoid the PG position, it was considered that the fabrication of circumferential welding is best done in two steps, i.e., by producing two separate welds on the circumference. To incorporate a two-stage welding cycle into the entire circumference of the joint, welding start and stop procedures were introduced and successfully tested, increasing and decreasing the welding energy linearly over time.

It should be emphasized that the set level of penetration requirement pushes used welding process near to the threshold in terms of weld pool controllability. The edge joint does not provide inherent support to the melt pool laterally, so the accuracy of electrode/torch alignment with respect to the joint is clearly important. Therefore, the position and orientation of the electrode/torch must be kept as optimal and constant as possible to avoid lateral drift of the melt. However, experiments evaluating the overall performance of the welding process showed that there was some tolerance for to the accuracy of the electrode/torch alignment. It was found that the welding process withstands a combined variation of + 0.5 mm from the optimal stand-off distance and a 5-degree deviation from the optimal orientation of the electrode angle as well as a 0.5 mm vertical misalignment at the weld joint.

Welding distortions observed in welding experiments with curved L-shaped specimens caused a welding torch setting error relative to a predetermined welding path that had been taught to the robot prior to welding. The torch alignment error caused by the welding distortions, in turn, led to an asymmetry in the weld cross-sectional profile where the weld had solidified at an angle of about 30-40 degrees from the vertical direction of the weld joint. The mentioned tilting of the cross-sectional profile of the weld resulted in insufficient penetration (typical values were 2-2.5 mm) in the direction of the joint. The occurrence of welding distortions in long circumferential welds is inevitable in applications with a lot to be welded, i.e., long welds. Therefore, it is recommended to use a seam tracking system integrated in the welding head attached to the wrist of the robot. The seam tracking system help the progress of welding by making the necessary position corrections to the tool center point (TCP), i.e., the tip of the electrode, by compensating for the position error caused by the welding distortions relative to the original predetermined position information.

Declaration of Competing Interest

The authors declare that they have no known competing financial interests or personal relationships that could have appeared to influence the work reported in this paper.

Acknowledgements

The authors would like to acknowledge the ITER Organization (IO) and VTT Technical Research Centre of Finland Ltd. for the permission to publish the results.

References

- [1] Mohandas T et al., 1999, A comparative evaluation of gas tungsten and shielded metal arc welds of a "ferritic" stainless steel, *J. Mater. Process. Technol.*, 94:133-140.
- [2] Moi SC et al., 2019, Design optimization of TIG welding process for AISI 316L stainless steel, *International Journal of Recent Technology and Engineering (IJRTE)*, 8 (2):5348-5354.
- [3] Serindağ HT, Çam G, 2021, Microstructure and mechanical properties of gas metal arc welded AISI 430/AISI 304 dissimilar stainless steels butt joints, *Journal of Physics: Conference Series*, 1777: 012047. <https://doi.org/10.1088/1742-6596/1777/1/012047>.
- [4] James F. Key, *Arc Physics of Gas-Tungsten Arc Welding*, ASM INTERNATIONAL, 1993, ASM Handbook, Volume 6, Welding Brazing and Soldering. ISBN 0-87170-377-7(V.1).
- [5] Massoud Goodarziy et al., 1997, The effect of the cathode tip angle on the GTAW arc and weld pool: I. Mathematical model of the arc. *J. Phys. D: Appl. Phys.* 30 (1997) 2744–2756.
- [6] Massoud Goodarziy et al., 1998, The effect of the cathode tip angle on the gas tungsten arc welding arc and weld pool: II. The mathematical model for the weld pool. *J. Phys. D: Appl. Phys.* 31 (1998) 569–583.
- [7] Shaik Himam Saheb and Chandrashekhhar A., 2019, Experimental study on influence of filler rods in gas Tungsten Arc welding. *AIP Conference Proceedings* 2166, 020007 (2019), <https://doi.org/10.1063/1.5131594>.
- [8] Régis Henrique Gonçalves e Silva et al., 2018, TIG welding process with dynamic feeding: a characterization approach. *The International Journal of Advanced Manufacturing Technology* (2018) 96:4467–4475 <https://doi.org/10.1007/s00170-018-1929-6>.
- [9] Kamlesh Kumar et al., 2021, A review on TIG welding technology variants and its effect on weld geometry. *Materials Today: Proceedings*, Article in press.
- [10] N., Karunakaran, 2012, Effect of Pulsed Current on Temperature Distribution, Weld Bead Profiles and Characteristics of GTA Welded Stainless Steel Joints. *International Journal of Engineering and Technology* Volume 2 No.12, December, 2012.
- [11] Taraneh Reza Tabrizi et al., 2021, Comparing the effect of continuous and pulsed current in the GTAW process of AISI 316L stainless steel welded joint: microstructural evolution, phase equilibrium, mechanical properties and fracture mode. *Journal of Materials Research and Technology* 2021;15:199–212.
- [12] A. Traidia et al., 2010, Optimal parameters for pulsed gas tungsten arc welding in partially and fully penetrated weld pools. *International Journal of Thermal Sciences* 49 (2010) 1197–1208.
- [13] P. K. Giridharan and N. Murugan, 2009, Optimization of pulsed GTA welding process parameters for the welding of AISI 304L stainless steel sheets. *Int J Adv Manuf Technol* (2009) 40:478–489, DOI 10.1007/s00170-008-1373-0.
- [14] Małgorzata Ostromęcka and Andrzej Kolasa, 2019, The effect of the current pulsation frequency on heat supply results during pulsed current TIG welding in 301L stainless steel. *Welding Technology Review*, Vol. 91(8) 2019, DOI: <http://dx.doi.org/10.26628/wtr.v91i8.1046>.
- [15] Z. Wang et al., 2010, Measurement and Estimation of Weld Pool Surface Depth and Weld Penetration in Pulsed Gas Metal Arc Welding. *Welding Journal* June 2010, Vol. 89 117–126.
- [16] Arivarasu, M. et al., 2014, Comparative Studies of High and Low Frequency Pulsing on the Aspect Ratio of Weld Bead in Gas Tungsten Arc Welded AISI 304L Plates. *Procedia Engineering* 97 (2014) 871–880.
- [17] G., Lothongkum, 1999, TIG pulse welding of 304L austenitic stainless steel in flat, vertical and overhead positions. *Journal of Materials Processing Technology* 89–90 (1999) 410–414.
- [18] Ahmet Durgutlu, 2003, Experimental investigation of the effect of hydrogen in argon as a shielding gas on TIG welding of austenitic stainless steel. *Materials and Design* 25 (2004) 19–23, <https://doi.org/10.1016/j.matdes.2003.07.004>.
- [19] J., Tusek, M., Suban, 2000, Experimental research of the effect of hydrogen in argon as a shielding gas in arc welding of high-alloy stainless steel. *International Journal of Hydrogen Energy* 25 (2000) 369–376.

- [20] Dipali Pandya et al., 2021, Effect of hydrogen additions to shielding gas on activated TIG austenitic stainless steel weld. *Materials Today: Proceedings* Volume 47, Part 4, 2021, Pages 1025-1029.
- [21] Gaurav Dak et al., 2020, Autogenous welding of copper pipe using orbital TIG welding technique for application as high vacuum boundary parts of nuclear fusion devices. *International Journal of Pressure Vessels and Piping* 188 (2020) 104225, <https://doi.org/10.1016/j.ijpvp.2020.104225>.
- [22] Ting Lei et al., 2021, The development of tube-to-tubesheet welding from automation to digitization. *The International Journal of Advanced Manufacturing Technology* (2021) 116:779–802, <https://doi.org/10.1007/s00170-021-07379-7>.
- [23] Ramesh Kumar Buddu et al., 2014, Mechanical properties and microstructural investigations of TIG welded 40 mm and 60 mm thick SS 316L samples for fusion reactor vacuum vessel applications. *Fusion Engineering and Design* 89 (2014) 3149–3158, <http://dx.doi.org/10.1016/j.fusengdes.2014.10.006>.
- [24] Laurent Foresta et al., 2018, The European ITER Test Blanket Modules: Fabrication R&D progress for HCLL and HCPB. *Fusion Engineering and Design* 136 (2018) 1408–1416, <https://doi.org/10.1016/j.fusengdes.2018.05.026>.
- [25] Zhirong Zhang et al., 2019, Qualification of the Weld for ITER PF6 Coil Tail. *IEEE Transactions on Applied Superconductivity*, Vol. 29, No. 7, October 2019.